Energies **2014**, *7*, 5332-5356; doi:10.3390/en7085332

OPEN ACCESS

energies

ISSN 1996-1073

www.mdpi.com/journal/energies

Article

Contribution of Vertical Methane Flux to Shallow Sediment Carbon Pools across Porangahau Ridge, New Zealand

Richard B. Coffin [1,†,*], Leila J. Hamdan [2], Joseph P. Smith [3], Paula S. Rose [4,†], Rebecca E. Plummer [5], Brandon Yoza [6], Ingo Pecher [7] and Michael T. Montgomery [1]

[1] Naval Research Laboratory, Washington, DC 20375, USA; E-Mail: michael.montgomery@nrl.navy.mil

[2] Department of Environmental Science and Policy, George Mason University, Fairfax, VA 22030, USA; E-Mail: lhamdan1@gmu.edu

[3] United States Naval Academy, Annapolis, MD 21402, USA; E-Mail: jpsmith@usna.edu

[4] Naval Research Laboratory, National Research Council, Washington, DC 20375, USA; E-Mail: paula.rose@tamucc.edu

[5] Department of Geology, University of Maryland College Park, College Park, MD 20742, USA; E-Mail: rplummer@umd.edu

[6] Hawaii Natural Energy Institute, University of Hawaii, Honolulu, HI 96822, USA; E-Mail: byoza@hawaii.edu

[7] School of Environment, University of Auckland, Auckland 1142, New Zealand; E-Mail: i.pecher@auckland.ac.nz

[†] Current Address: Department of Physical and Environmental Sciences, Texas A&M University—Corpus Christi, Corpus Christi, TX 78412, USA.

[*] Author to whom correspondence should be addressed; E-Mail: richard.coffin@tamucc.edu; Tel.: +1-361-825-2456.

Received: 12 June 2014; in revised form: 4 August 2014 / Accepted: 11 August 2014 / Published: 18 August 2014

Abstract: Moderate elevated vertical methane (CH_4) flux is associated with sediment accretion and raised fluid expulsion at the Hikurangi subduction margin, located along the northeast coast of New Zealand. This focused CH_4 flux contributes to the cycling of inorganic and organic carbon in solid phase sediment and pore water. Along a 7 km offshore transect across the Porangahau Ridge, vertical CH_4 flux rates range from 11.4 $mmol \cdot m^{-2} \cdot a^{-1}$ off the ridge to 82.6 $mmol \cdot m^{-2} \cdot a^{-1}$ at the ridge base. Stable carbon isotope ratios ($\delta^{13}C$) in pore water and sediment were variable across the ridge suggesting close proximity of heterogeneous

carbon sources. Methane stable carbon isotope ratios ranging from −107.9‰ to −60.5‰ and a C1:C2 of 3000 indicate a microbial, or biogenic, source. Near ridge, average $\delta^{13}C$ for pore water and sediment inorganic carbon were ^{13}C-depleted (−28.7‰ and −7.9‰, respectively) relative to all core subsamples (−19.9‰ and −2.4‰, respectively) suggesting localized anaerobic CH_4 oxidation and precipitation of authigenic carbonates. Through the transect there was low contribution from anaerobic oxidation of CH_4 to organic carbon pools; for all cores $\delta^{13}C$ values of pore water dissolved organic carbon and sediment organic carbon averaged −24.4‰ and −22.1‰, respectively. Anaerobic oxidation of CH_4 contributed to pore water and sediment organic carbon near the ridge as evidenced by carbon isotope values as low as to −42.8‰ and −24.7‰, respectively. Carbon concentration and isotope analyses distinguished contributions from CH_4 and phytodetrital carbon sources across the ridge and show a low methane contribution to organic carbon.

Keywords: coastal sediment; carbon cycling; methane; phytodetritus; convergence forcing; stable isotopes

1. Introduction

The majority of coastal sediment carbon cycling studies have focused on contributions from autochthonous photosynthetic marine and allocthonous terrigenous inputs [1–3]. However, hydrocarbons produced within deep sediment through thermochemical and microbiological conversions can significantly contribute to cycling of carbon, especially in shallower sediments and water column [4–9]. Stable carbon isotope ratios ($\delta^{13}C$) indicative of petroleum and methane (CH_4) origins are found in bacterioplankton biomarkers [4]. In a related study in the Northeastern Pacific Ocean, it has been estimated that sediment methane contributes about 28% of the carbon to the water column dissolved organic carbon (DOC) pool [10,11] and is a significant energy resource for biological activity in many coastal regions worldwide [10,12–14]. Methane also contributes to carbon pools within shallow sediments [13,15,16].

Vertical CH_4 flux in shallow sediments is predominantly controlled by anaerobic oxidation of methane (AOM) which occurs at the sulfate-methane transition (SMT) zone [17–20]. Equation (1) shows the net biochemical reaction for AOM in marine sediments:

$$CH_4 + SO_4^{2-} \rightarrow HCO_3^- + HS^- + H_2O \quad (1)$$

Comparison of SMT depths in CH_4-rich sediments through different marine environments suggests a wide range in vertical CH_4 flux rates that are dependent on CH_4 concentrations and physical settings [16,21–23].

Natural abundance carbon isotopes have been useful for studying microbial cycling of hydrocarbons in marine environments [4,5,24–27]. Stable carbon isotope analysis ($\delta^{13}C$) of CH_4 has been successfully used to distinguish between thermogenic and biogenic CH_4 sources [28,29]. Furthermore, $\delta^{13}C$ values of pore water dissolved inorganic carbon (DIC) and calcium carbonate ($CaCO_3$) can provide an assessment of AOM and/or CH_4 reduction through methanogenesis [14,30–32]. Vertical CH_4 fluxes combined

with carbon isotope analysis of organic and inorganic carbon pools in coastal ocean regions will help to quantify the contribution of CH_4 to the shallow sediment carbon pools.

Along the Hikurangi Margin, the Pacific Plate subducts beneath the Australian Plate at a rate of 40–45 mm·year^{-1} [33]. On the southern margin, sediment accretion occurs at a rate of approximately 12 mm·year^{-1} [34] and subduction creates a focused vertical fluid flux from deep within the accretionary wedge and underthrust sediments [35]. In this study, the relative contribution of CH_4 from subducting sediments and pelagic phytodetritus to shallow sediment is examined using $\delta^{13}C$ values of solid phase sediment and pore water carbon pools (Figure 1). Focused fluid advection, observed immediately adjacent to the landward flank of the ridge, may contribute to carbon shallow sediment carbon cycling, along with *ex situ* pelagic derived organic matter (terrestrial and pelagic sources) [35–37]. This study provides further assessment of previous seismic data interpretation. We test the hypothesis that the different sources of carbon, CH_4 and pelagic detritus, partition between dissolved and particulate carbon pools with CH_4 as the primary contributor to pore water dissolved carbon and pelagic detritus the dominant contributor to sediment carbon (Figure 2).

Figure 1. Sediment core locations across the Porangahau Ridge on the Hikurangi Margin, east of northern New Zealand.

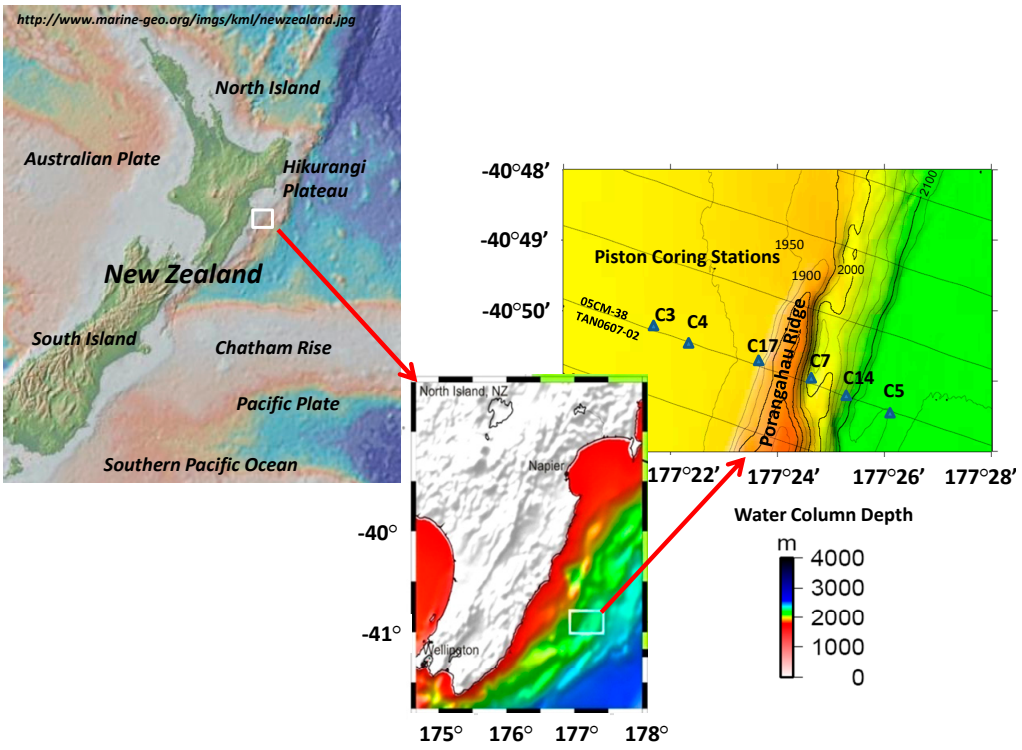

2. Methods

2.1. Regional Description

The Hikurangi Plateau is an igneous province within the Pacific Plate, undergoing oblique subduction below the Australian Plate [33], leading to formation of an accretionary wedge 20–25 Ma ago [34]. The central Hikurangi subduction margin contains a 150 km wide imbricated frontal wedge that is poorly drained and over pressured with low taper thrust systems concurrent with a smooth subducting

plate, a thick trench sedimentary sequence, and weak basal décollement with a convergent rate of approximately 40 mm·a^{-1} [38]. The Porangahau Ridge is located south on this subduction margin on the outer accretionary wedge (Figure 1). Sediment geology at this location is driven by the accretionary wedge growing at a rapid rate, filling with turbidites and mudstones [34].

Bottom simulating reflections (BSR) in seismic profiles through large areas of this study region indicate the presence of gas hydrates [39,40]. A local heatflow anomaly based on upwarping of BSRs was interpreted as an indication of fluid expulsion from the subduction interface on the Porangahau Ridge [35]. Previous work suggests that gas from beneath the Porangahau Basin in the accretionary wedge is transported along with fluids that undergo a compaction during sediment subduction and possibly transform from a smectite to illite (Figure 2). Fluid is interpreted to migrate horizontally along a décollement that transition to a vertical pattern through a thrust fault upon downward décollement stepping or vertical hydrofracturing [40]. A high-resistivity anomaly on the western landward side of the ridge if due to gas hydrates would provide further evidence for elevated fluid flow [36].

Figure 2. Sediment and pore water carbon pools studied across the Porangahau Ridge to determine the relative contribution of phytodetritus and vertical CH_4 flux to shallow sediment. Sediment organic and inorganic carbon concentrations (SOC and $CaCO_3$) and $\delta^{13}C$ (SOC and TIC) and pore water dissolved organic and inorganic carbon (DOC and DIC) are summarized to compare spatial variation in these carbon sources. Data interpretation suggests phytodetritus dominates contribution to solid phase sediment carbon while AOM has a more significant contribution to the dissolved carbon cycling which, subsequently, contributes to the solid phase pool.

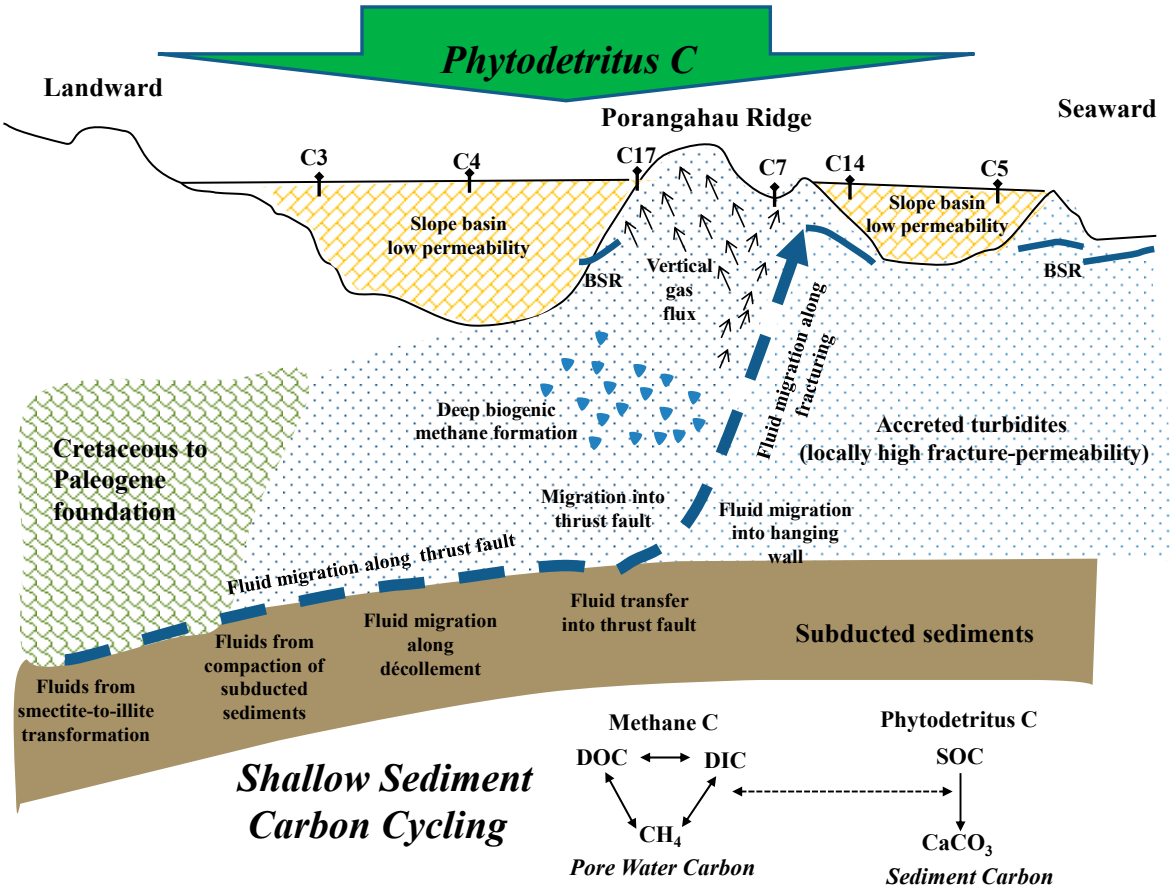

Seismic data retrieved during hydrocarbon exploration across the Porangahau Ridge displayed strong reflections above the predicted regional BSR; profiles were interpreted as free gas beneath a locally upwarped base of gas hydrate stability zone. These data were used to focus piston coring locations for this study. The coring area is seaward of a Cretaceous to Palaogene base believed to create a deforming tectonic buttress for a frontal accretionary wedge comprised of underlying Plio- to Pleistocene accreted turbidites that are near slope basins formed the Miocene to recent times [38,41]. Six cores were collected in June 2006 across the ridge in an offshore transect (Figure 1) [36,37]. Data were interpreted to compare variation in the contribution of CH_4 and pelagic detritus to shallow system carbon pools across the ridge with previous indications of fluid expulsion at specific locations along this transect [35] (Figure 2).

2.2. Sample Collection and Analysis

Sediment was collected using a 6.5 m piston core with an average of 15 subsamples taken from each core; cores ranged in length from 206 to 480 centimeters below sea floor (cmbsf). Pore water was obtained using Reeburgh style presses pressurized to ~400 kPa (~60 psi) [36,37].

For determination of sediment CH_4 and higher molecular weight gas concentrations, a sediment plug was collected from the core using a 3 mL syringe with the end removed and sealed a in 20 mL serum vial. Gas was extracted [42] and measured on-board using a Shimadzu GC-FID GC-14A gas chromatograph equipped with a 6 foot Hayesep-Q 80/100 mesh column (Alltech, Deerfield, IL, USA) and quantified with certified gas standards (Scott Gas, Plumbsteadville, PA, USA). Limit of detection (LOD) for CH_4 concentrations was 0.009 mM; values below LOD are presented as 0.0 mM.

A Dionex DX-120 ion chromatograph (Thermo Scientific, Waltham, MA, USA) was used on-board to measure pore water SO_4^{2-} concentrations. Samples were diluted 1:50 (vol:vol^{-1}) prior to analysis and measured against IAPSO (International Association for the Physical Sciences of the Ocean) standard seawater (28.9 mM SO_4^{2-}). The SO_4^{2-} LOD was 0.6 mM; values below LOD are reported as 0.0 mM.

Total dissolved sulfide (TDS) concentrations were measured on-board using a Turner spectrophotometer [43]. LOD was 0.05 mM; values below LOD are reported as 0.0 mM.

Concentrations of DIC were measured on-board using a coulometer (UIC, Inc., Joliet, IL, USA) that was standardized with a certified reference material (CRM #68, Scripps, La Jolla, CA, USA). LOD for DIC was 0.23 mM. DIC concentrations in all samples were above LOD.

Sediment samples were stored frozen in pre-weighed snap-tight Petri dishes. Porosity was determined from wet and dry mass of sediment. Concentrations and stable carbon isotopic compositions of sediment organic carbon (SOC) and total carbon (TC) were determined with a Thermo Delta Plus XP IRMS (Thermo Scientific, Waltham, MA, USA) in-line with a Costech EA using a Conflo III interface and helium carrier gas. Fifteen to 20 mg of dry, homogenized sediment was analyzed in triplicate. For SOC, sediments were weighed into silver capsules, acidified with excess 10% HCl to remove inorganic carbon, and dried at 60 °C. For TC, sediments were weighed into tin capsules and analyzed with no further treatment. Percent calcium carbonate (%$CaCO_3$) was determined by subtracting %SOC from the %TC. Sediment $\delta^{13}C_{TIC}$, was calculated using a mass and isotopic balance.

Stable carbon isotope ratios ($\delta^{13}C$) were measured on TC, SOC, CH_4, dissolved organic carbon (DOC) and DIC. $\delta^{13}C_{CH4}$ was measured from the same samples used for CH_4 concentrations; samples

with concentrations less than 2 μM are similar to the atmospheric background and are not reported. A sufficient volume of headspace was first cryogenically concentrated [44], and subsequently introduced into a Thermo Trace gas chromatograph (GC) equipped with a Varian Porapak-Q column, interfaced via a GC-C III combustion interface to a Thermo Delta Plus XP IRMS.

The same GC-C-IRMS system, with a split/splitless inlet instead of the cryofocusing unit, was used to measure $\delta^{13}C_{DIC}$ [13]. One mL of pore water was sealed in a 2 mL serum vial, then acidified with 20 μL of 85% phosphoric acid to convert the DIC to CO_2, which was then extracted into the headspace and injected into the GC.

$\delta^{13}C_{DOC}$ was analyzed using an OI Analytical 1010 wet chemical oxidation system (OI Analytical, College Station, TX, USA) in line with the IRMS [45]. All $\delta^{13}C$ data are presented in per mil units (‰), and referenced to the PeeDee Belmenite standard.

2.3. Carbon Pool Data Interpretation

Data was evaluated assuming that carbon cycling associated with AOM is oxidation of CH_4 to CO_2 and fixation of CO_2 into microbial biomass [46]. AOM contribution to sediment carbon pools was studied assuming mixing between two end-members: phytodetritus (C_{PD}) and CH_4 (C_{CH_4}). The spatial variation in the CH_4 contribution to sediment carbon pools through the study region is evaluated with mass and isotopic balances summarized by Equations (2) and (3):

$$C_x = C_{PD} + C_{CH_4} \tag{2}$$

$$\delta^{13}C_xC_x = \delta^{13}C_{PD}C_{PD} + \delta^{13}C_{CH_4}C_{CH_4} \tag{3}$$

where C_x = concentration of the carbon pool ($CaCO_3$, SOC, DOC and DIC) and $\delta^{13}C_x$ = the stable isotopic composition of the respective component. During diagenesis of organic matter with the initial components $C_{PD(i)}$ and $C_{CH4(i)}$, mass and isotopic changes of carbon pools are represented by Equation (4):

$$\delta^{13}C_xC_x = \delta^{13}C_{PD}C_{PD(i)} + \delta^{13}C_{CH_4}C_{CH_4(i)} + \delta^{13}C_{\Delta}\Delta C \tag{4}$$

where ΔC = net change in carbon pool concentration and $\delta^{13}C_{\Delta}$ = net change in isotopic composition during diagenesis. When $\delta^{13}C_{PD}C_{PD}$ (or $\delta^{13}C_{CH4}C_{CH4}$) = constant or zero and $\Delta C_x \neq$ zero, Equation (5) becomes:

$$\frac{d(\delta^{13}C \times C)}{dC} = \delta^{13}C_{\Delta} + \frac{d(\delta^{13}C_{\Delta})}{dC}\Delta C \tag{5}$$

where linear slopes of $\delta^{13}C_xC_x$ *versus* C_x estimate the net isotopic signal of carbon lost or gained through vertical sediment profiles during diagenesis [47–50].

The relative contribution of AOM to carbon pools at key depths, through each sediment core, was calculated using a two end-member isotope mass balance [51]:

$$R_X = R_{PD}C_{PD} + R_{CH_4}C_{CH_4} \tag{6}$$

where R_X represents the isotopic composition ($\delta^{13}C$) of the C pools: DIC, TIC, DOC and SOC, R_{PD} and R_{CH4} represent the isotopic composition of marine phytodetritus (PD) and CH_4 respectively, and C_{PD} and C_{CH4} represent their corresponding fractional contributions such that:

$$C_{PD}+C_{CH_4}=1 \quad (7)$$

Percent contribution of CH_4 to each C pool (%X) is derived from Equations (6)–(8):

$$\%X=\frac{R_X-R_{PD}}{R_S-R_{PD}}\times 100 \quad (8)$$

where R_s represents the isotopic composition of CH_4 or DIC.

3. Results

Measured CH_4 concentrations ranged from LOD to 11.4 mM (Figure 3). The lowest concentrations were furthest off the ridge in both the landward and seaward direction, whereas the highest were at the landward ridge base (C17). All CH_4 profiles had lowest concentrations in shallowest core sections. Concentrations in ridge cores (C17 and C7) showed rapid increases at mid core depths (Figure 3). $\delta^{13}C_{CH4}$ values ranged from −107.9‰ to −60.5‰ (Figure 3). Generally, $\delta^{13}C_{CH4}$ profiles were more positive (^{13}C-enriched) in shallow sediment and more negative (^{13}C-depleted) down core. Strong ^{13}C-depletion occurred mid depth in C4, C17, and C7 (Figure 3). Average C1:C2 was 3000 (n = 23) and combined with the range of $\delta^{13}C_{CH4}$ values, indicates a biogenic CH_4 source in this region.

Pore water SO_4^{2-} concentrations ranged from the LOD in mid to deep core sections to 29.3 mM in near surface sediments (Figure 4). Minimum SO_4^{2-} concentration in each core was observed at different depths, with C17 and C7 having SO_4^{2-} depletion at the most shallow depths. TDS ranged from LOD to 11.9 mM (Figure 4). TDS was not detected in surface sediments and increased down core in the presence of rapid shifts in CH_4 and SO_4^{2-} profiles. Highest H_2S concentrations were observed in C17 and C7.

Pore water DIC values ranged from 2.5 mM to 21.5 mM (Figure 5). Except in C3, profiles showed low concentrations in surface samples and rapid non-conservative concave up increases at mid core depths (Figure 5). In C3, collected closest to shore, average DIC concentrations were lowest overall. In all cores $\delta^{13}C_{DIC}$ values ranged from 3.0‰ to −47.6‰ with consistent ^{13}C-enrichments in surface sediments (Figure 5). Seaward off the ridge (C5 and C14) $\delta^{13}C_{DIC}$ profiles were linear with down core shifts to minimum values: –27.6‰ and –31.6‰, respectively. In contrast, $\delta^{13}C_{DIC}$ profiles for C4, C17 and C7 were sharply ^{13}C-depleted to a minimum of −45.1‰ (C7, Figure 5). In C3 there was a smaller range in δ^{13}C values between the shallow and deep pore water samples (−5.3‰ to −20.1‰).

Sediment $CaCO_3$ concentrations ranged from 5.9% to 32.3% (Figure 6). With the exception of C17 and C7, all cores had relatively uniform $CaCO_3$ profiles with a range of 5.9% to 17.0% coupled with slight variation in $\delta^{13}C_{TIC}$ profiles (−3.5‰ to 1.3‰). In contrast, in C17%$CaCO_3$ ranged from 5.9% to 32.3%, with the highest percentage 156 cmbsf (Figure 6). Concomitant with the $CaCO_3$ increase in C17, there was ^{13}C depletion (Figure 6).

Sediment porosity ranged from 0.477 to 0.766 and averaged 0.604 ± 0.059 (n = 53). Across the ridge core, %SOC ranged from 0.24% to 0.85% (Figure 7) and was lowest in cores closest to the ridge (C17 and C7). The $\delta^{13}C_{SOC}$ values ranged from −19.0‰ to −24.7‰ and were generally enriched in surface sediment and depleted at depth toward the SO_4^{2-} minimum; a trend that was most apparent in C17 (Figure 7).

Pore water DOC concentrations ranged from 0.3 mM to 5.2 mM, with core average concentrations lowest in C17 and highest in C4 and C14 (Figure 8). Pore water $\delta^{13}C_{DOC}$ values ranged from −42.8‰

to −21.1‰, suggesting variation in DOC sources. In C3, C7 and C5, $\delta^{13}C_{DOC}$ varied approximately ±2‰ through the profiles (Figure 8).

Figure 3. Profiles of sediment CH_4 concentrations and $\delta^{13}C$ values relative to centimeters below seafloor (cmbsf) from piston cores collected across the Porangahau Ridge. Graphs are listed by location relative to the ridge with the first column westward moving to the ridge and the second column eastward moving off the ridge.

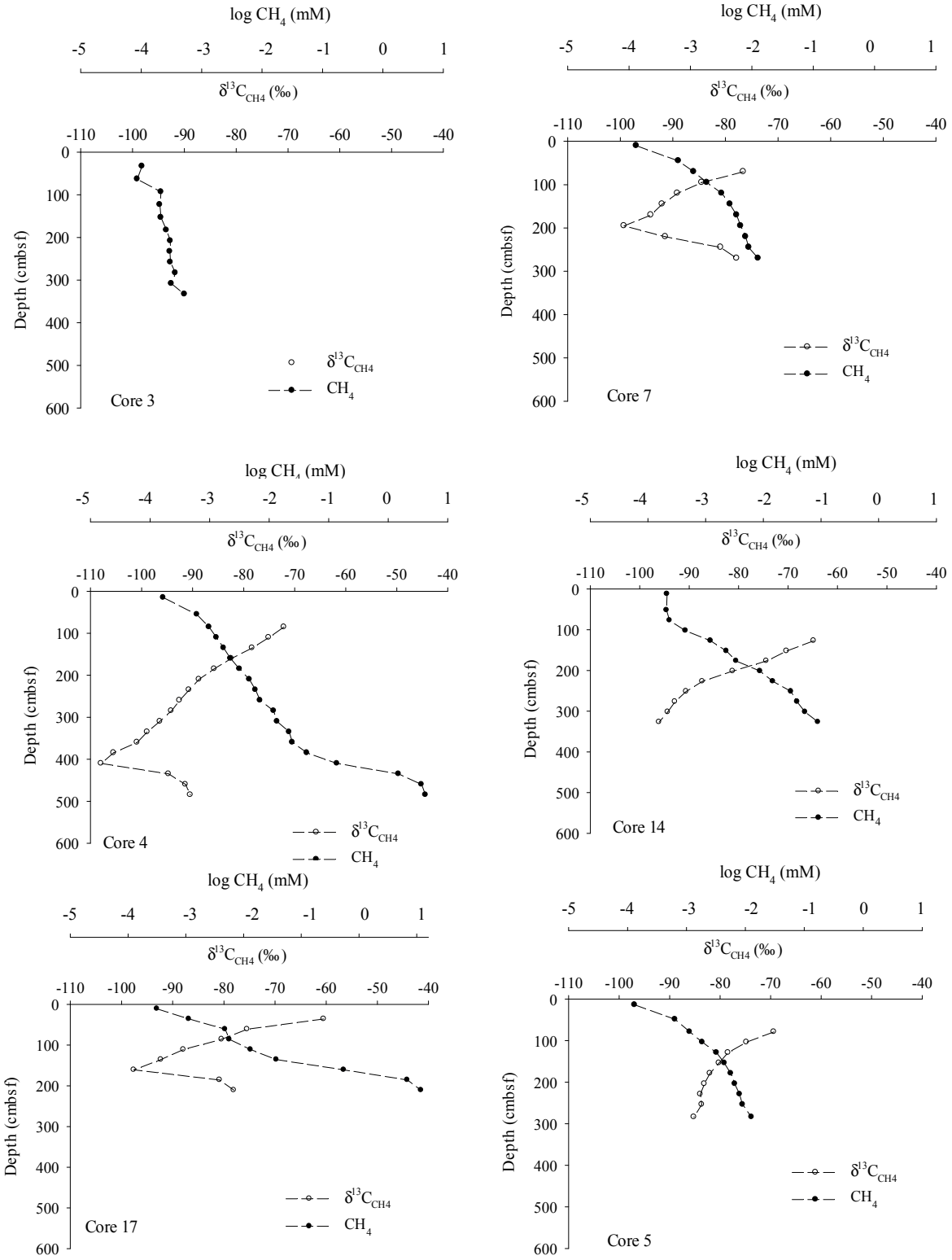

Figure 4. Profiles of pore water SO_4^{2-} (●) and TDS (○) concentrations in piston cores relative to centimeters below seafloor (cmbsf) collected across the Porangahau Ridge. Lines are drawn through the linear portion of the SO_4^{2-} profile that were used to estimate the sulfate-methane transition (SMT) depth (cmbsf) and the diffusive SO_4^{2-} (and CH_4) flux (mmol $SO_4^{2-} \cdot m^{-2} \cdot a^{-1}$). Graphs are listed by location relative to the ridge with the first column westward moving to the ridge and the second column eastward moving off the ridge.

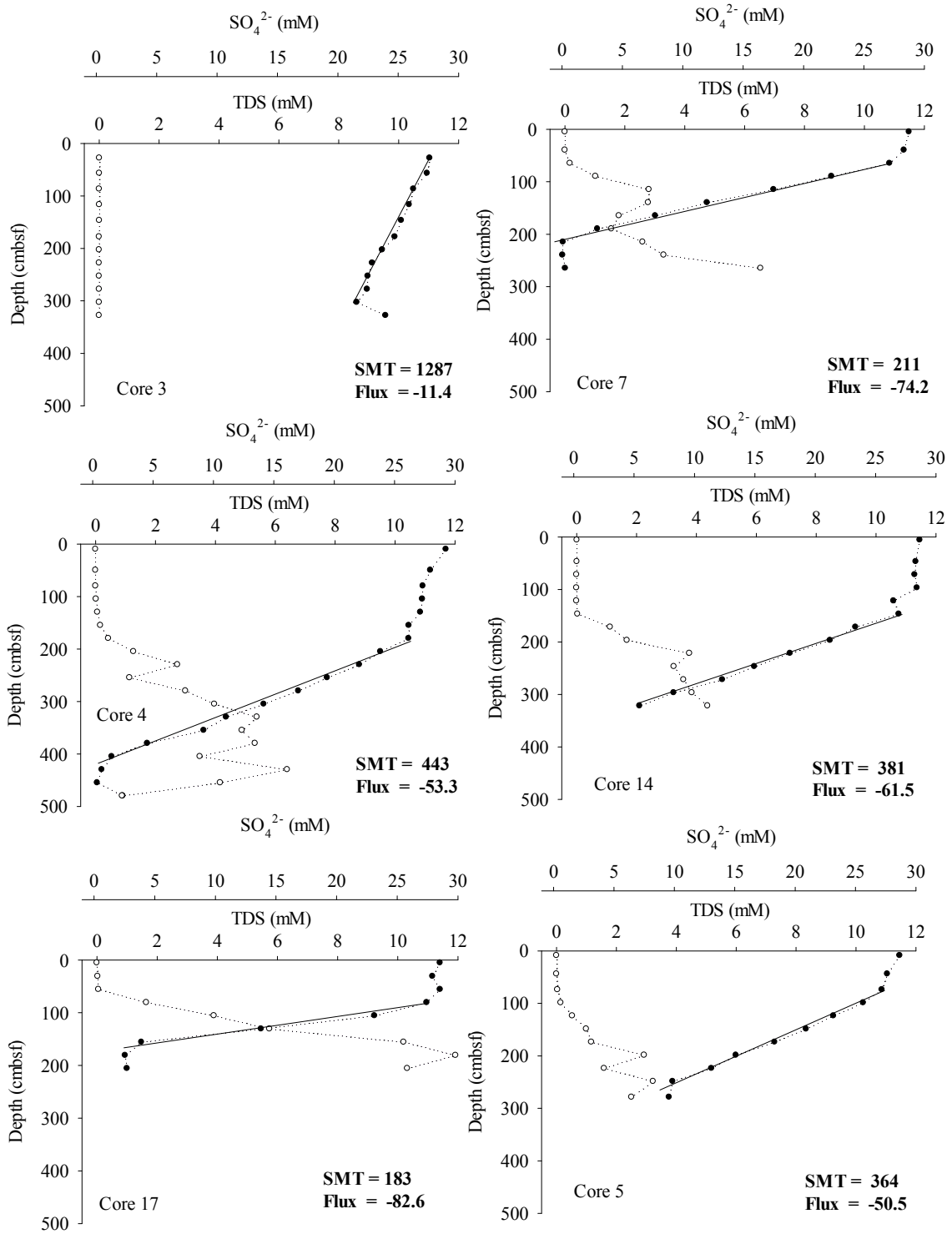

Figure 5. Profiles of pore water dissolved inorganic carbon (DIC) concentrations and $\delta^{13}C$ values relative to centimeters below seafloor (cmbsf) in piston cores collected across the Porangahau Ridge. Graphs are listed by location relative to the ridge with the first column westward moving to the ridge and the second column eastward moving off the ridge.

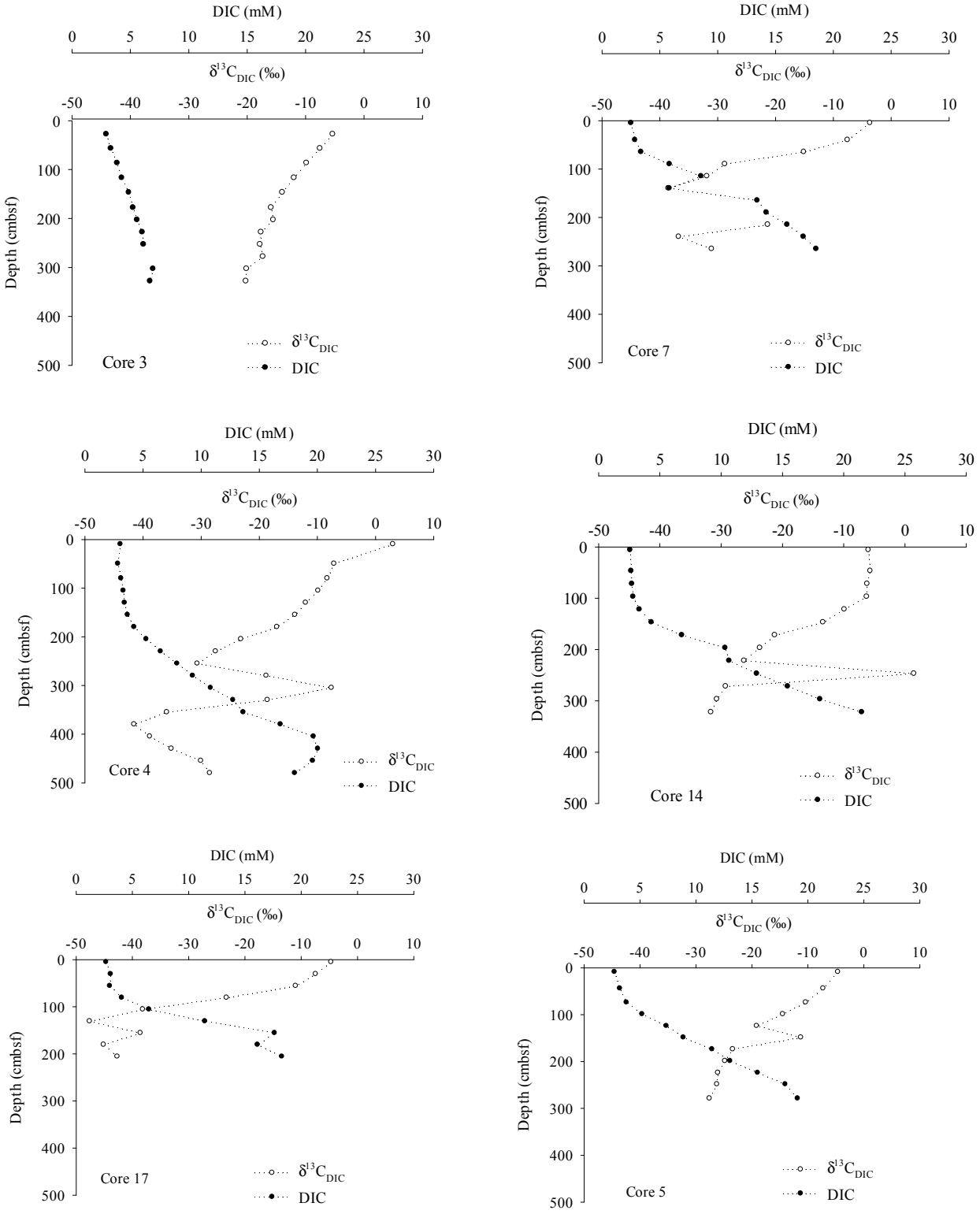

Figure 6. Profiles of sediment percent $CaCO_3$ and $\delta^{13}C$ values of the total inorganic carbon ($CaCO_3$) relative to centimeters below seafloor (cmbsf) in piston cores collected across the Porangahau Ridge. Graphs are listed by location relative to the ridge with the first column westward moving to the ridge and the second column eastward moving off the ridge.

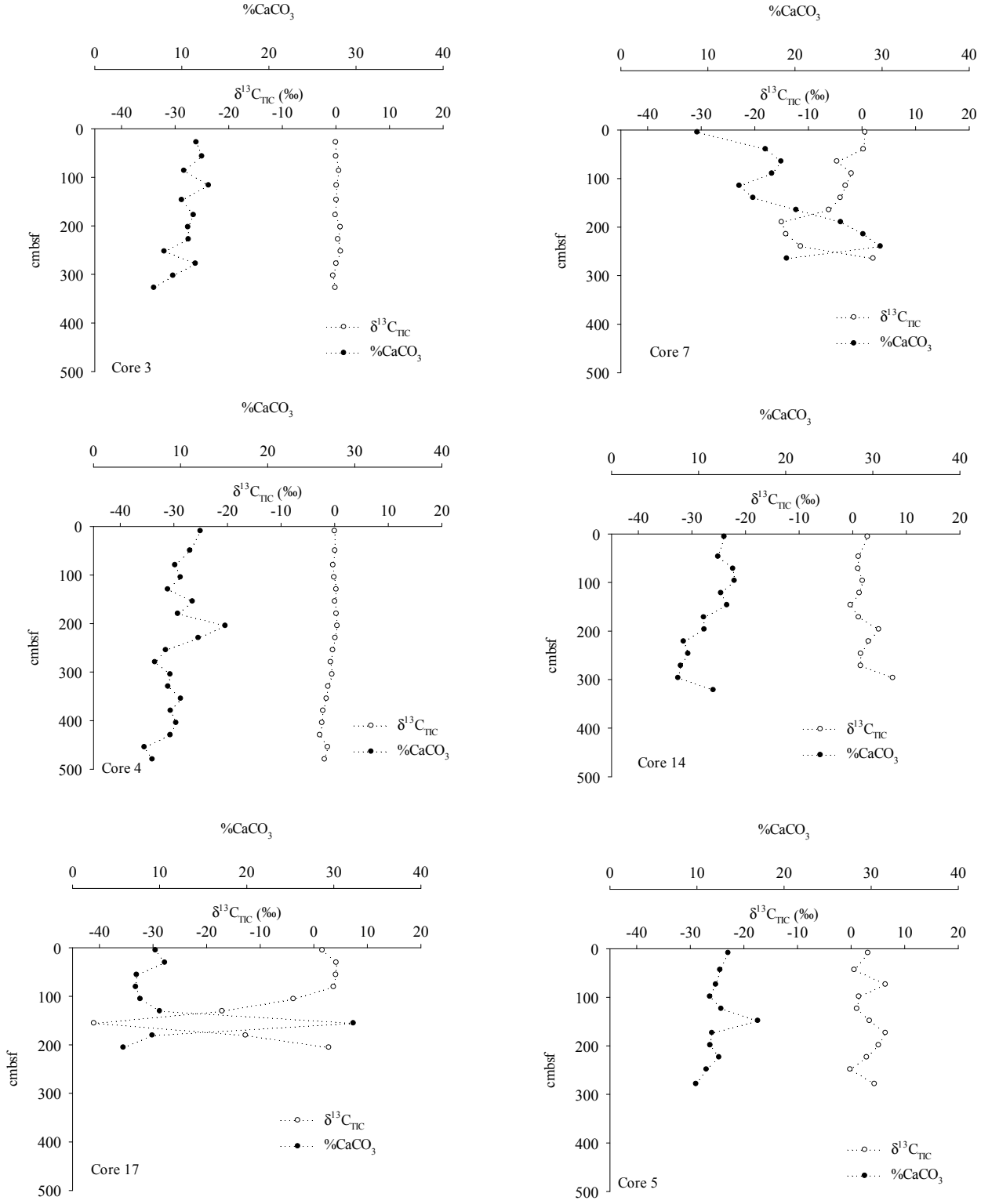

Figure 7. Profiles of percent (%C) and $\delta^{13}C$ values of sediment organic carbon (SOC) relative to centimeters below seafloor (cmbsf) in piston cores collected across the Porangahau Ridge. Graphs are listed by location relative to the ridge with the first column westward moving to the ridge and the second column eastward moving off the ridge.

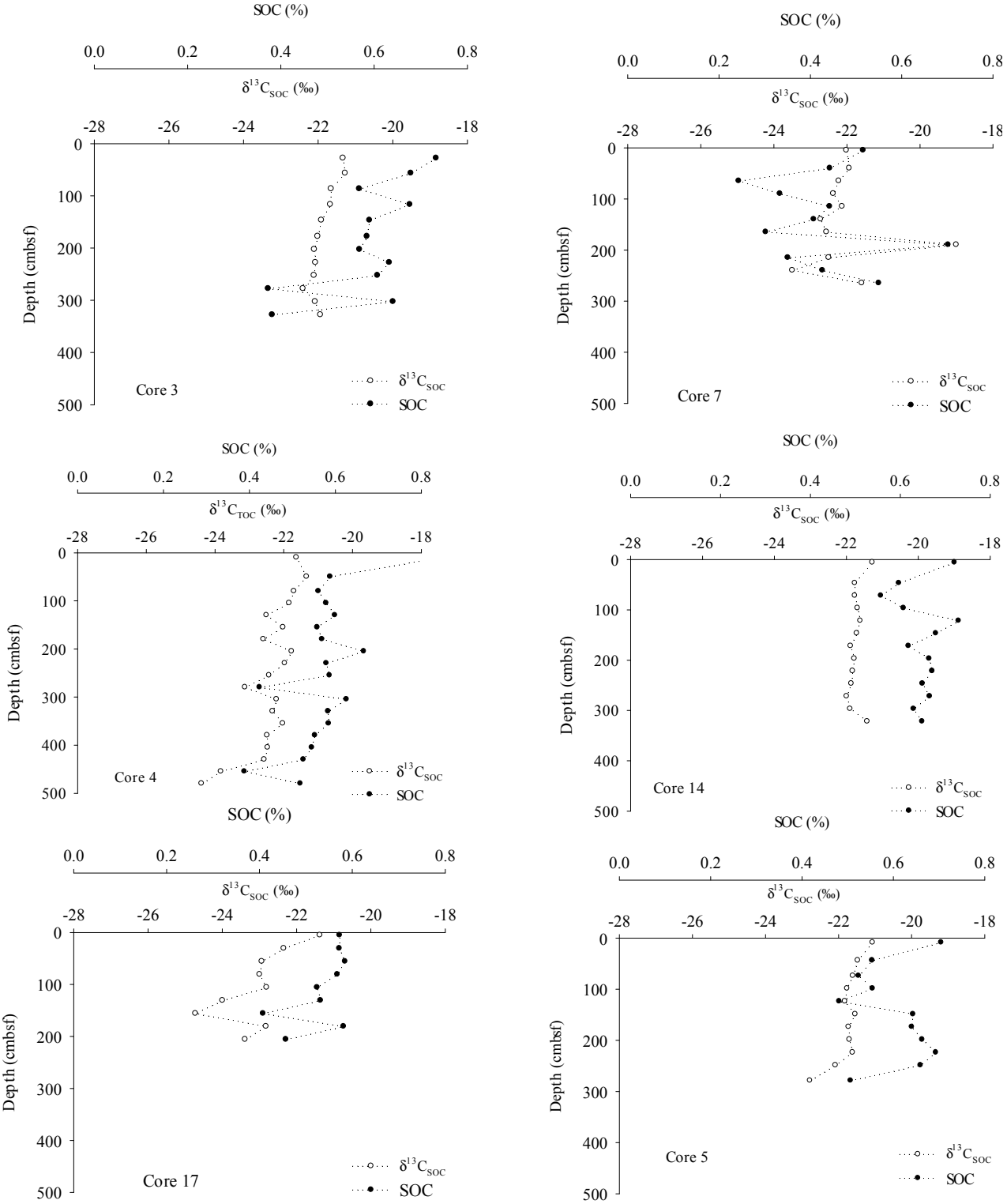

Figure 8. Profiles of pore water dissolved organic carbon (DOC) concentrations and $\delta^{13}C$ values relative to centimeters below seafloor (cmbsf) in piston cores collected across the Porangahau Ridge. Graphs are listed by location relative to the ridge with the first column westward moving to the ridge and the second column eastward moving off the ridge.

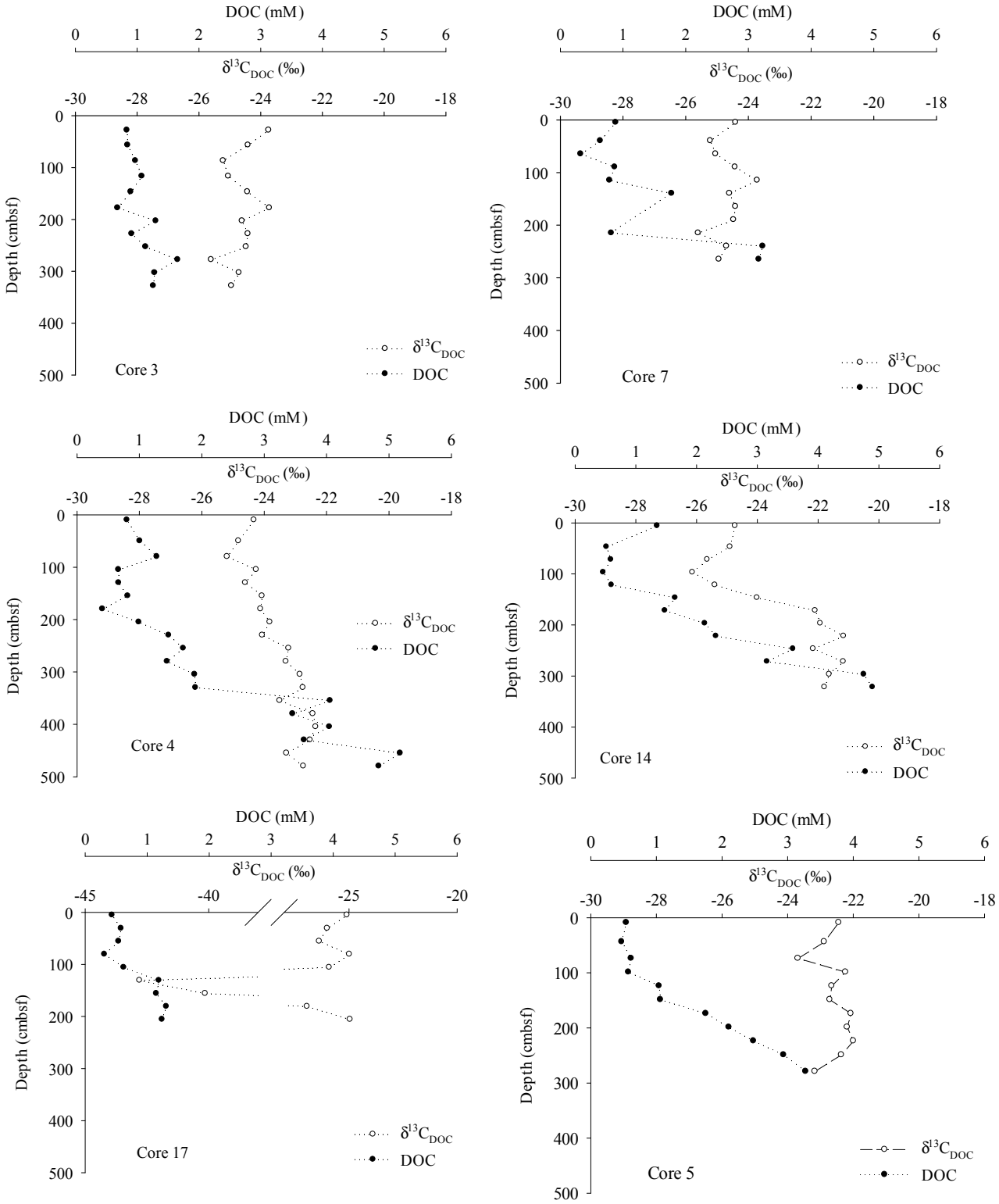

4. Discussion

4.1. Methane Source, Vertical Flux and Cycling

Measured stable carbon isotope ratios and gas compositions are typical of biogenic CH_4 ($\delta^{13}C_{CH4}$ = −107.9‰ to −60.5‰; average C1:C2 = 3000, [29]). In general, CH_4 concentrations decrease with distance away from the ridge (Figure 3). Concentration profiles reflect active CH_4 consumption via AOM at mid core depths and CH_4 production below this zone (Figures 3 and 4). Elevated TDS and DIC concentrations coincide with increasing CH_4 and decreasing SO_4^{2-} concentrations which suggest AOM is the principle process controlling sediment CH_4 profiles (Equation (1), Figures 4 and 5). Isotopic fractionation during AOM and methanogenesis is evident in the $\delta^{13}C_{CH4}$ and $\delta^{13}C_{DIC}$ profiles. During AOM ^{13}C-depleted CO_2 is produced and subsequent reduction of this CO_2 results in a $\delta^{13}C_{CH4}$ minimum at the SMT as observed in C4, C17 and C7 ([21,52–54]; Figure 3; Figure 5). AOM signature is most prominent in C4, C17 and C7 where $\delta^{13}C_{DIC}$ values are more ^{13}C-depleted. Furthermore, the bacterial phylotypes commonly observed to participate in sulfate dependent AOM were observed in these sediments [37].

SMT depth is primarily a function of vertical CH_4 flux [18]. Although sediment did appear to contain low SOC concentrations (Figure 7) there is potential for organoclastic SO_4^{2-} reduction in the shallow sediment where small changes in concentrations were observed (Figure 4; [55]). Linear portions of SO_4^{2-} profiles indicated consumption of CH_4 by AOM (Figure 4). An absence of TDS in shallow sediments may occur because of oxidation by bio-irrigation, but there is a clear pattern of TDS production correlated with linear declines in pore water SO_4^{2-} concentrations through the SMT resulting from AOM (Figure 4). Linear SO_4^{2-} profiles were extrapolated to estimate SMT depth and indicated that C17 and C7 had shallowest SMT zones at 183 and 211 cmbsf, respectively (Figure 4). Deepest SMT (1287 cmbsf) was in nearshore C3, well off the ridge. In the other cores, SMT zones were at intermediate depths (364–443 cmbsf).

Assuming steady state consumption and the reaction stoichiometry of AOM (Equation (1)), CH_4 fluxes were estimated using SO_4^{2-} profiles and Fick's First Law [17,56]. Highest CH_4 fluxes were on the ridge in C17 and C7 (86.2 and 74.2 mmol $m^{-2}\cdot a^{-1}$, respectively). Off ridge CH_4 flux rates were lower, ranging from 11.4 to 61.5 mmol $m^{-2}\cdot a^{-1}$, with higher values offshore (Figure 4). Methane fluxes across Porangahau Ridge are moderate relative to values reported for other coastal regions. Similar ranges have been reported for passive sediment regions in the Bering, Kara, Chukchi and White Seas with maximum values at 25.3 and 47.4 mmol CH_4 $m^{-2}\cdot a^{-1}$ [21,22]. However, regions in the Beaufort Sea with past accumulation of scoured sediment show elevated CH_4 fluxes at 154.8 mmol CH_4 $m^{-2}\cdot a^{-1}$ [16]. Higher diffusion rates at 249 mmol CH_4 $m^{-2}\cdot a^{-1}$, reported across a mound in Atwater Valley on the Texas-Louisiana Shelf, may be the result of deep sediment hydrate instability caused by salt diapirs [13]. On the mid Chilean Margin, with extreme plate subduction, geochemical profiles at a seismic blanking region showed an elevated flux at 362 mmol CH_4 $m^{-2}\cdot a^{-1}$ [15]. While seismic data and presence of a high-resistivity anomaly on the western side of the Porangahau Ridge indicates fluid migration resulting from décollement or vertical hydrofracturing [35,36], geochemical estimates of deep CH_4 migration to shallow sediments suggest lower CH_4 hydrate loading relative to other coastal locations.

4.2. Inorganic Carbon Pools in Porangahau Ridge Sediments

Solid phase sediment and pore water inorganic carbon concentrations and $\delta^{13}C$ values are influenced by microbial processes (AOM, OSR, and methanogenesis) and physical properties (downward diffusion and carbon pool solubility). In deeper core sections, increases in DIC concentration associated with decreases in SO_4^{2-} concentration are attributed to elevated AOM rates (Figure 4). DIC profiles were generally concave up at mid core depths, being most pronounced in C17 (Figure 5). Concave up concentration profiles suggest that DIC production from AOM is greater than DIC losses from diffusion and carbonate precipitation [57]. These data support the conservative interpretation of observed vertical CH_4 fluxes and AOM.

DIC concentrations and $\delta^{13}C_{DIC}$ profiles reflect variation in vertical CH_4 flux across the ridge (Figure 5). Steepest gradients in DIC concentrations and the most ^{13}C-depleted $\delta^{13}C_{DIC}$ values were near the ridge in C17 and C7 and also in C4, landward further from the ridge. Vertical CH_4 flux is most rapid at C17 relative to other locations. Minimum $\delta^{13}C_{DIC}$ values at the SMT (−43.3‰ to −47.5‰) that are more ^{13}C-depleted than resident organic matter (−24.5‰ ± 0.5‰, Figure 7) are unequivocal evidence of AOM [58–60]. In addition, there is a mid-profile, rapid enrichment in ^{13}C that we assume results from shallow sediment CH_4 production (Figure 5). Slight decreases in DIC concentrations are associated with shifts in the $\delta^{13}C_{DIC}$ at C7 and C17.

Authigenic $CaCO_3$ concentrations and ^{13}C-depleted pore water DIC suggest elevated AOM rates at the SMT [46,58]. ^{13}C-enriched DIC in C4, C17 and C7, below the SMT results from isotopic fractionation during CO_2 reduction [54,61]. In C3 $\delta^{13}C_{DIC}$ values range from −5.3‰ (a near seawater value) to −20.2‰ at the greatest core depth. $\delta^{13}C$ values of sediment organic matter are conserved during microbial respiration to DIC [27,31,61,62]. Average $\delta^{13}C_{SOC}$ value through C3 is −21.7‰ ± 0.3‰ (n = 12, Figure 7). Such a shift in $\delta^{13}C_{DIC}$ may result from mixing between seawater and microbially-respired phytodetritus. This location is used later in this discussion as a phytodetritus end-member for calculating the CH_4 contribution to DIC pools across the ridge.

Active CH_4 cycling is also reflected in $CaCO_3$ and $\delta^{13}C_{TIC}$ profiles in near ridge cores C17 and C7 (Figure 6). Increased carbonate alkalinity as a result of AOM precipitates $CaCO_3$ and incorporates ^{13}C-depleted DIC into this pool [30]. Calcium carbonate ranged 5.9% to 32% of solid phase sediment. Off ridge cores (C3, C4, C14, and C5) had relatively uniform $CaCO_3$ and $\delta^{13}C_{TIC}$ profiles with depth in the sediment. A strong contrast to this was observed in C17 with a maximum $CaCO_3$ concentration (32.3% at 156 cmbsf) and a minimum $\delta^{13}C_{TIC}$ value at the same depth (−43.8‰). Similar $CaCO_3$ and $\delta^{13}C_{TIC}$ profiles were observed at C7. These $CaCO_3$ and $\delta^{13}C_{TIC}$ profiles highlight locations where CH_4 contribution to bulk carbon pools is greatest.

4.3. Organic Carbon Pools in Porangahau Ridge Sediments

Methane cycling is not reflected to the same extent in SOC profiles (Figure 7). Sediment organic carbon concentrations were lowest in ridge cores (C17 and C7) and increased off the ridge. Range of $\delta^{13}C_{SOC}$ values across the ridge suggests two carbon sources: phytodetritus and CH_4 (−19.0‰ to −24.7‰). In the most landward core (C3), $\delta^{13}C_{SOC}$ profiles were relatively uniform and had values characteristic of phytodetritus (−22.5‰ to −18.7‰, [27,63,64]). In other cores, $\delta^{13}C_{SOC}$ values were

generally ^{13}C-enriched in surface sediments and ^{13}C-depleted at depth. A recent study nearby on southern Wairarapa Ridge reported $\delta^{13}C_{SOC}$ values in near surface sediment (<10 cmbsf) ranging from −22.8‰ to −22.3‰ in seep locations and non-seep (control) sites [63]. This illustrates that despite high CH_4 fluxes in this region, CH_4 was not appreciably incorporated into the SOC pool.

In this study, phytodetritus is the predominant source of SOC in most cores. However, an alternate source of SOC was observed in deep sections of C4 and C17 with a minimum $\delta^{13}C_{SOC}$ value at C17 (−24.7‰). Although these values approach terrestrially-derived carbon signatures [62], considering the distance offshore, overlying ^{13}C-enriched SOC, pore water DIC concentration and $\delta^{13}C_{DIC}$ profiles, this is likely from CH_4 cycling. Note that ^{13}C-depletion of SOC is concomitant with lower SOC concentrations in C17 suggesting decreased organic carbon production associated with CH_4 cycling. Similar shifts in $\delta^{13}C_{SOC}$ values with depth were not observed in a location close to our study site [63]; however, this may be a function of their sampling depth (≤10 cm) relative to the SMT depth.

Pore water DOC concentrations showed similar patterns to SOC with the lowest concentrations in C17 and higher in C4 (Figure 8). In C17, lower CH_4 concentration corresponded to pronounced ^{13}C-depletion in $\delta^{13}C_{DOC}$ (−42.8‰). Of note is the disparate range of $\delta^{13}C_{DOC}$ values encountered in surface sediment across the ridge and ^{13}C-depletion in DOC at mid depths in C17. In the case of C4 and C14, an increase in concentration was accompanied by a ^{13}C-enrichment in DOC. In C17, DOC was significantly ^{13}C-depleted near and at the SMT (156 cmbsf, respectively) where DOC concentrations were lower.

Other studies indicate CH_4 contributes to pore water DOC. At a Gulf of Mexico site with advective CH_4 flux (−3250 mM $m^{-1} \cdot a^{-1}$), there was substantial depletion of $\delta^{13}C_{DOC}$ (−27.6‰) which reflected influence of AOM in this carbon pool [13,65]. In contrast, on the Cascadia Margin, average $\delta^{13}C_{DOC}$ values were −21.6‰ ± 1.3‰ in a region with active advective methane fluxes [32]. Enriched $\delta^{13}C_{DOC}$ suggests advection of CH_4 prohibits AOM and subsequent production of DOC. However, a sediment CH_4 source to the Cascadia Margin water column contributed 28% of water column DOC in a region with an advective flux [10].

4.4. Methane Contribution to Shallow Sediment Carbon Pools

Carbon mass and isotope balances in each vertical core profile indicate CH_4 contribution to carbon cycling varies across the ridge (Equations (2)–(5); Figure 2). Linear slopes of $\delta^{13}C_xC_x$ *versus* C_x reflect the net isotopic signature of carbon lost or gained at each site in the various pools. Sites at the ridge base have ^{13}C-depleted values, consistent with AOM and methanogenesis (Table 1). Net isotopic value ($\delta^{13}C_\Delta$) of pore water DIC ranged from −31.4‰ to −35.0‰ off the ridge. Near the ridge, $\delta^{13}C_\Delta$ values of DIC were lower below the SMT in C4 and C7 (−49.2‰ to −41.3‰), and through the entire C17 profile (−48.8‰). For TIC, $\delta^{13}C_\Delta$ values ranged from 0.0‰ to 1.1‰ off the ridge at C3, C4, C14 and C5. Near the ridge at C17 and C7, $\delta^{13}C_\Delta$ values ranged from −58.0‰ to −22.6‰, with the most ^{13}C-depleted values in C17 suggesting a substantial AOM contribution to the carbon pool. Although AOM contribution to inorganic carbon pool is clearly evident, SOC $\delta^{13}C_\Delta$ values ranged from −21.2‰ to −17.1‰, indicating phytodetritus was the dominant source of sediment organic carbon. Pore water DOC $\delta^{13}C_\Delta$ values ranged from −40.9‰ to −21.1‰. In C17, a ^{13}C-depleted value of −40.9‰ suggests CH_4 contributed to the DOC pool below the SMT; above the SMT there was a moderate contribution

from phytodetritus with a slight ^{13}C-enrichment (−36.5‰). $\delta^{13}C_{\Delta}$ value for DOC was also depleted in C3 on the near shore, landward side of the ridge. However, $\delta^{13}C_{DIC}$ values and CH_4 flux estimates do not indicate a significant CH_4 contribution at this site. Here the ^{13}C-depleted value may indicate a recalcitrant source of terrestrial organic matter.

Table 1. Net isotopic values ($\delta^{13}C_{\Delta}$) calculated for dissolved inorganic carbon (DIC), organic carbon (DOC) and total inorganic carbon ($CaCO_3$) and sediment organic carbon (SOC) derived from the slopes of the plots $\delta^{13}C_x \times C_x$ *versus* C_x (Equation (5)). Data from C4, C17 and C7 were plotted above (A) and below (B) the SMT. Values for C3, C4 and C5 were generated from full core profiles.

Station	DIC	DOC	$CaCO_3$	SOC
	$\delta^{13}C_{\Delta}$			
C3	−31.4	−26.5	0.0	−20.8
C4 A	−31.6	−22.6	1.0	−19.5
B	−41.3	−22.3	1.1	−20.2
C17 A	−48.8	−36.5	−56.6	−17.8
B	−49.2	−40.9	−58.0	−17.1
C7 A	−33.4	−22.8	−22.6	−21.2
B	−46.6	−22.6	−23.0	−21.6
C14	−35.0	−21.1	0.8	−20.6
C5	−31.4	−22.6	0.0	−20.3

Further examination of CH_4 contribution to sediment carbon cycling was conducted with a two-end-member isotope mass balance [51]. It was assumed that CH_4 is not directly assimilated, but is first oxidized via AOM and the CO_2 (DIC) produced in this reaction is fixed into biomass [46]. This assumption is supported by research showing the AOM community only assimilates 1% of the CH_4 with the other 99% being oxidized to CO_2. Subsequently, a significant proportion of CH_4 sourced CO_2 is assimilated by the AOM community [66–68]. Assimilation of CH_4 carbon through AOM contrasts with aerobic CH_4 oxidation where 60% of CH_4 carbon is assimilated into biomass [69].

AOM contribution to SOC, $CaCO_3$, DOC and DIC was estimated in C4, C17 and C7, where an SMT was observed, using a carbon isotope mass balance (Equations (6)–(8)). CH_4 contribution to each carbon pool was estimated at the SMT (*i.e.*, the maximum contribution in each core). Regarding SOC, a ^{13}C isotopic fractionation of −3.75‰ during CO_2 fixation was assumed, a midpoint for the 2.0‰ to 5.5‰ range expected for the reversed tricarboxylic acid cycle (rTCA) [70–72]. This assumption is based on extensive data gathered for rTCA in laboratory and field research where bacterial biomass results in $\delta^{13}C$ values to be −2.0‰ to −12.0‰ depleted relative to the substrate through a temperature range of 30–100 °C and varying growth conditions [70–74]. Characterization of the microbial community diversity in sediments supports the assumption that the primary CO_2 fixation cycle is rTCA [75,76]. Selection of an intermediate value (−3.75‰) is based on core samples taken from sediment profiles at points where AOM was active and low isotope fractionation during CO_2 assimilation is expected. To evaluate AOM contribution to SOC ($\%SOC_{CH4}$), the average $\delta^{13}C_{SOC}$ value of C3 as the C_{PD} end-member was used (−21.7‰, Table 2). This value is within the expected range of water column phytoplankton: −22.5‰ to −18.7‰ [27,63,64,77,78]. Low CH_4 concentrations and a near conservative

DIC concentration and $\delta^{13}C_{DIC}$ profiles suggest minimal CH_4 contribution to carbon cycling in this core and support the use of this end-member. For C17, with assumptions stated above, the δ^{13}Cend-members for DIC (−47.6‰) and phytodetritus (−21.7‰) and minimum $\delta^{13}C_{SOC}$ value in the SMT (−24.7‰) AOM contribution to SOC is 8%. Using the same approach for C4 and C7 and end members listed in Table 2, the contributions of AOM to SOC are 12% and 8%, respectively (Table 3).

Table 2. δ^{13}C values (‰) used in carbon isotope mass balance calculations to estimate CH_4 contribution to sediment organic carbon (SOC), dissolved inorganic carbon (DIC), total inorganic carbon (TIC) and dissolved organic carbon (DOC). Sample data are the minimum values observed in the sulfate-methane transition zone. End-members used are phytodetritus (PD), methane (CH_4) and dissolved inorganic carbon (DIC). Note: ***** indicates values to which the −3.75‰ fractionation was applied for isotopic mass balance calculations.

Core	SOC			$CaCO_3$			DOC			DIC		
	End members		Samples	End members		Samples	End members		Samples	End members		Samples
	PD	DIC *	SOC	PD	CH4	TIC	PD	DIC *	DOC	PD	CH4	DIC
C4	−21.7	−41.5	−24.4	−0.3	−83.3	−2.7	−21.7	−41.5	−23.3	−21.7	−83.3	−41.5
C17	−21.7	−47.6	−24.7	−0.3	−83.3	−43.9	−21.7	−47.6	−42.8	−21.7	−83.3	−47.6
C7	−21.7	−38.5	−23.4	−0.3	−83.3	−15.0	−21.7	−38.5	−26.6	−21.7	−83.3	−38.5

To estimate AOM contribution to $CaCO_3$, it was assumed that there was no isotopic fractionation during DIC precipitation to form $CaCO_3$ [79]. $\delta^{13}C_{TIC}$ profile in C3 did not vary with depth, showed no evidence of CH_4, and had a relatively conservative DIC profile. Thus, we used the average $\delta^{13}C_{TIC}$ value from C3 (−0.3‰) as the phytodetritus end-member for estimating contribution of CH_4 to the $CaCO_3$ pool. The CH_4 end-member is the average $\delta^{13}C_{CH4}$ value below the SMT from all cores (−83.3‰). For C17, the minimum $\delta^{13}C_{TIC}$ value (−43.9‰, Table 2) observed through the SMT represents a 55% contribution from AOM (Table 3). In C7, the AOM contribution to $CaCO_3$ was estimated to be 19% based on a $\delta^{13}C_{TIC}$ of −15.0‰. Moving landward to C4, the minimum $\delta^{13}C_{TIC}$ value of −2.5‰ resulted in a CH_4 contribution to $CaCO_3$ of 3%.

Table 3. Percent CH_4 contribution to dissolved inorganic carbon (DIC), dissolved organic carbon (DOC), calcium carbonate ($CaCO_3$), and sediment organic carbon (SOC) at core locations observed to have a SMT (C4, C17, C7).

Core	DIC	DOC	$CaCO_3$	SOC
C4	32%	7%	3%	12%
C17	47%	71%	55%	8%
C7	33%	24%	19%	8%

For CH_4 contribution to sediment pore water carbon pools, it was assumed that phtyodetritus-derived $\delta^{13}C_{DOC}$ was −21.7‰ and that DOC is produced during DIC fixation; therefore the same DIC end-members as in SOC calculations were used (Table 2). With these end-members and a $\delta^{13}C_{DOC}$ value of −42.8‰, maximum AOM contribution to DOC is 71% in C17 (Table 3). Moving seaward to C7, contribution of AOM to pore water DOC was estimated to be 24%. Landward in C4, the AOM contribution to DOC was 7%.

To calculate CH_4 contribution to pore water DIC, the CH_4 end-member presented above for $CaCO_3$ (−83.3‰) was used with no isotopic fractionation. The phytodetritus end-member was estimated using C3 pore water $\delta^{13}C_{DIC}$ profile (Figure 4). $\delta^{13}C_{DIC}$ values in C3 represent mixing of seawater DIC (~0‰) and DIC derived from SOC degradation (−21.7‰) were used, with no contribution from CH_4. For C17 and C7, the phytodetritus end-member is the $\delta^{13}C_{DIC}$ value in C3 at respective depths of the SMT (C17 = −15.9‰ at 183 cmbsf; C7 = −16.5‰ at 211 cmbsf). Using the same approach for C4 and extrapolating the C3 profile to 443 cmbsf (the depth of the SMT in C4) resulted in a $\delta^{13}C_{DIC}$ value that cannot be representative of mixing between DIC derived from seawater and that derived from SOC degradation (−32.2‰). Therefore, −21.7‰ was used for the phytodetritus end-member, a reasonable value for DIC produced during SOC decomposition. In C17 the minimum $\delta^{13}C_{DIC}$ value in the SMT was −47.6‰; CH_4 was estimated to contribute 47% to the DIC pool (Table 3). In C7, $\delta^{13}C_{DIC}$ at the SMT is −38.5‰ resulting in a 33% contribution from CH_4 to DIC. In C4, maximum contribution from AOM is 32% to pore water DIC.

5. Conclusions

Relative contribution of phytodetritus and deep biogenic CH_4 to shallow sediment carbon pools varies across the Porangahau Ridge. Estimated CH_4 fluxes across the ridge ranged from 11.4 to 86.2 mmol CH_4 $m^{-2}\cdot a^{-1}$ with the highest value on the westward side of the ridge where heat flow, seismic and controlled source electromagnetics data indicate elevated vertical fluid migration [35,36]. While seismic and geophysical parameters do show high fluid migration, CH_4 flux at this study site is moderate relative to previous studies [13,15]. These data do show need for a combination of seismic and geochemical data for a thorough assessment of vertical methane flux levels. A carbon mass and isotope evaluation through core profiles [47,48] showed strong variation in contribution of CH_4 to SOC, $CaCO_3$, DOC and DIC (Table 1). A key observation for this assessment is the westward ridge elevated CH_4 contribution to $CaCO_3$ and DIC but not to SOC. A large contribution to $CaCO_3$ but not SOC results from low microbial biomass production relative to CH_4 oxidation. There was CH_4 contribution to pore water DOC, but DOC concentrations are 3-fold lower than SOC resulting in a low contribution to the total carbon. At locations with an observed SMT (C4, C17 and C7) a more thorough evaluation of the CH_4 contribution to shallow sediment carbon cycling is completed with a two end-member isotope mass balance [51]. At the landward ridge location (C17), CH_4 contribution to $CaCO_3$ and DIC was 55% and 47%, respectively showing a high respiration of CH_4 to inorganic carbon pools during AOM (Table 3**)**. There was a large contribution of AOM to pore water DOC at this location (71%); however, as stated above, this is small fraction of total sediment carbon. The CH_4 contribution to SOC in this location was only 8%. In contrast, at C4 CH_4 contribution to CaCO3 and DIC was 3% and 32%, indicating lower values of CH_4-sourced carbon precipitating to inorganic phases. CH_4-sourced pore water DOC at this location was an order of magnitude less (7%). Off ridge sediment is dominated by phytodetritus. This study examines shallow sediment carbon cycling and highlights the need to assess deep sediment CH_4 contribution to coastal models. In addition, the combination of sediment geochemical profiles, seismic data [35], CSEM, and estimates of vertical fluid migration [36] provides strong predictive tools of for deep sediment CH_4 hydrate loadings.

Acknowledgments

Acknowledgment is made to the New Zealand Foundation of Research, Science and Technology, Office of Naval Research and Department of Energy, National Energy Technology Laboratory for financial support of this research. We express sincere appreciation for support from the *RV Tangaroa* crew for support during this expedition.

Author Contributions

All authors have contributed to writing and revisions of this manuscript.

Conflicts of Interest

The authors declare no conflict of interest.

References

1. Milliman, J. Flux and fate of fluvial sediment and water in coastal seas. In *Ocean Margin Processes in Global Change*; Mantoura, R.F.C., Martin, J., Wollast, R., Eds.; Wiley: New York, NY, USA, 1991; pp. 69–90.
2. Goñi, M.A.; Ruttenberg, K.C.; Eglinton, T.I. Sources and contribution of terrigenous organic carbon to surface sediments in the Gulf of Mexico. *Nature* **1997**, *389*, 275–278.
3. Mayer, L.M.; Schick, L.L.; Allison, M.A.; Rutthenberg, K.C.; Bentley, S.J. Marine *vs.* terrigenous organic matter in Louisiana coastal sediments: The uses of bromine:organic carbon ratios. *Mar. Chem.* **2007**, *107*, 244–254.
4. Kelley, C.A.; Coffin, R.B.; Cifuentes, L.A. Stable isotope evidence for alternate carbon sources in the Gulf of Mexico. *Limnol. Oceanogr.* **1998**, *43*, 1962–1969.
5. Wang, X.-C.; Chen, R.F.; Whelan, J.; Eglinton, T. Contribution of "old" carbon from natural marine hydrocarbon seeps to sedimentary and dissolved organic carbon pools in the Gulf of Mexico. *Geophys. Res. Lett.* **2001**, *28*, 3313–3316.
6. Joye, S.B.; Boetius, A.; Orcutt, B.N.; Montoya, J.P.; Schulz, H.N.; Erickson, M.J.; Lugo, S.K. The anaerobic oxidation of methane and sulfate reduction in sediments from Gulf of Mexico cold seeps. *Chem. Geol.* **2004**, *205*, 219–238.
7. Paull, C.K.; Ussler, W., III; Lorenson, T.; Winters, W.; Dougherty, J. Geochemical constraints on the distribution of gas hydrates in the Gulf of Mexico. *Geol. Mar. Lett.* **2005**, *25*, 273–280.
8. Ruppel, C.; Dickens, G.R.; Castellini, D.G.; Gilhooly, W.; Lizarralde, D. Heat and salt inhibition of gas hydrate formation in the northern Gulf of Mexico. *Geophys. Res. Lett.* **2005**, *32*, doi:10.1029/2004GL021909.
9. Lapham, L.L.; Chanton, J.P.; Martens, C.S.; Sleeper, K.; Woolsey, J.R. Microbial activity in surficial sediments overlying acoustic wipeout zones at a Gulf of Mexico cold seep. *Geochem. Geophy. Geosyst.* **2008**, *9*, doi:10.1029/2008GC001944.
10. Pohlman, J.W.; Bauer, J.E.; Waite, W.F.; Osburn, C.L.; Chapman, N.R. Methane hydrate-bearing seeps as a source of aged dissolved organic carbon to the oceans. *Nat. Geosci.* **2011**, *4*, 37–41.

11. McCarthy, M.D.; Beaupré, S.R.; Walker, B.D.; Voparil, I.; Guilderson, T.P.; Druffel, E.R.M. Chemosynthetic origin of ^{14}C-depleted dissolved organic matter in a ridge-flank hydrothermal system. *Nat. Geosci.* **2011**, *4*, doi:10.1038/NGEO1015.
12. Pohlman, J.W.; Kaneko, M.; Heuer, V.B.; Coffin, R.B.; Whiticar, M. Methane soucrces and production in the north Cascadia Margin gas hydrate system. *Earth Planet. Sci. Lett.* **2009**, *287*, 504–512.
13. Coffin, R.B.; Hamdan, L.; Plummer, R.; Smith, J.; Gardner, J.; Wood, W.T. Analysis of methane and sulfate flux in methane charged sediments from the Mississippi Canyon, Gulf of Mexico. *Mar. Petrol. Geol.* **2008**, *25*, 977–987.
14. Reitner, J.; Peckmann, J.; Reimer, A.; Schumann, G.; Thiel, V. Methane-derived carbonate build-ups and associated microbial communities at cold seeps on the lower Crimean shelf. (Black Sea). *Facies* **2005**, *51*, 66–79.
15. Coffin, R.B.; Pohlman, J.W.; Gardner, J.; Downer, R.; Wood, W.; Hamdan, L.; Walker, S.; Plummer, R.; Gettrust, J.; Diaz, J. Methane hydrate exploration on the mid Chilean coast: A geochemical and geophysical survey. *Am. Chem. Soc. Div. Pet. Chem.* **2007**, *56*, 32–41.
16. Coffin, R.B.; Hamdan, L.; Smith, J.P.; Plummer, R.; Millholland, L.; Larson, R. Spatial variation in shallow sediment methane source and cycling on the Alaskan Beaufort Sea. *Mar. Pet. Geol.* **2013**, *45*, doi:10.1016/j.marpetgeo.2013.05.002.
17. Borowski, W.S.; Paull, C.K.; Ussler, W., III. Marine porewater sulfate profiles indicate *in situ* methane flux from underlying gas hydrate. *Geology* **1996**, *24*, 655–658.
18. Borowski, W.S.; Paull, C.K.; Ussler, W., III. Global and local variations of interstitial sulfate gradients in the deep-water, continental margin sediments: Sensitivity to underlying methane and gas hydrates. *Mar. Geol.* **1999**, *159*, 131–154.
19. Orphan, V.J.; House, C.H.; Hinrichs, K.-U.; McKeegan, K.D.; DeLong, E.F. Methane-consuming archaea revealed by directly coupled isotopic and phylogenetic analysis. *Science* **2001**, *293*, 484–487.
20. Valentine, D.L. Biogeochemistry and microbial ecology of methane oxidation in anoxic environments: A review. *Antonie Leeuwenhoek* **2002**, *81*, 271–282.
21. Wehrmann, L.M.; Risgaard-Petersen, N.; Schrum, H.N.; Walsh, E.A.; Huh, Y.; Ikehara, M.; Pierre, C.; D'Hondt, S.; Ferdelman, R.G.; Ravelo, A.C.; *et al*. Couple organic and inorganic carbon cycling in the deep subseafloor sediment of the northeastern Bering Sea Slope (IODP Exp. 323). *Chem. Geol*. **2011**, *284*, 251–261.
22. Lein, A.Y.; Savvichev, A.S.; Ivanov, M.V. Reservoir of dissolved methand in the water column of the sea of the Russian Arctic region. *Doklady Earth Sci.* **2011**, *441*, 1576–1578.
23. Treude, T.; Niggemann, J.; Kallmeyer, J.; Wintersteller, P.; Schubert, C.J.; Boetius, A.; Jørgensen, B.B. Anaerobic oxidation of methane and sulfate reduction along the Chilean continental margin. *Geochim. Cosmochim. Acta* **2005**, *69*, 2767–2779.
24. Kessler, J.D.; Reeburgh, W.S.; Valentine, D.L.; Kinnaman, F.S.; Peltzer, E.T.; Brewer, P.G.; Southon, J.; Tyler, S.C. A survey of methane isotope abundance (^{14}C, ^{13}C, ^{2}H) from five nearshore marine basins that reveals unusual radiocarbon levels in subsurface waters. *J. Geophys. Res.* **2008**, *113*, doi:10.1029/2008JC004822.

25. Savvichev, A.S.; Rusanov, I.I.; Pimenov, N.V.; Pimenov, E.E.; Zakharova, E.E.; Veslopolova, E.F.; Lein, A.Y.; Crane, K.; Ivanov, M.V. Microbial processes of the carbon and sulphur cycles in the Chukchi Sea. *Microbiology* **2007**, *76*, 603–613.
26. Broecker, W.; Barker, S.; Clark, E.; Hajdas, I.; Bonani, G.; Stott, L. Ventilation of the glacial deep pacific ocean. *Science* **2004**, *306*, 1169–1172.
27. Wang, X.; Chen, R.F.; Gardner, G.B. Sources and transport of dissolved and particulate organic carbon in the Mississippi River estuary and adjacent coastal waters of the northern Gulf of Mexico. *Mar. Chem.* **2004**, *89*, 241–256.
28. Sassen, R.; MacDonald, I.R. Hydrocarbons of experimental and natural gas hydrates, Gulf of Mexico continental slope. *Org. Geochem.* **1997**, *26*, 289–293.
29. Milkov, A.V. Molecular and stable isotope compositions of natural gas hydrates: A revised global data set and basic interpretations in the context of geological settings. *Org. Geochem.* **2005**, *36*, 681–702.
30. Rodrigues, N.M.; Paull, C.K.; Borowski, W.S. Zonation of authigenic carbonates within gas hydrate-bearing sedimentary sections on the blake ridge: Offshore Southeastern North America. In *Proceedings of the Ocean Drilling Program—Scientific Results*; Paull, C.K., Matsumoto, R., Wallace, P.J., Dillon, W.P., Eds.; Ocean Drilling Program: College Station, TX, USA, 2000; Volume 164.
31. Chen, F.; Zhang, L.; Yang, Y.; Zhang, D. Chemical and isotopic alteration of organic matter during early diagenesis: Evidence from the coastal area off-shore the Pearl River estuary, south China. *J. Mar. Syst.* **2008**, *74*, 372–384.
32. Heuer, V.B.; Pohlman, J.W.; Torres, M.E.; Elvert, M.; Hinrichs, K.-U. The stable isotope biogeochemistry of acetate and other dissolved carbon species in deep subseafloor sediments at the northern Cascadia Margin. *Geochem. Cosmochim. Acta* **2009**, *73*, 3323–3336.
33. DeMets, C.; Gordon, R.G.; Argus, D.F.; Stein, S. Effect of recent revisions to the geomagnetic reversal time scale on estimates of current plate motions. *Geophys. Res. Lett.* **1994**, *21*, 2191–2194.
34. Barnes, P.M.; Mercier de Lépinay, B. Rates and mechanics of rapid frontal acrretion along the very obliquely converget southern Hikurangi Margin, New Zealand. *J. Geophys. Res.* **1997**, *102*, 24931–24952.
35. Pecher, I.A.; Henrys, S.A.; Wood, W.T.; Kukowski, N.; Crutchley, G.J.; Fohrmann, M.; Kilner, J.; Senger, K.; Gorman, A.R.; Coffin, R.B.; *et al*. Focussed fluid flow on the Hikurangi Margin, New Zealand—Evidence from possible local upwarping of the base fo gas hydrate stability. *Mar. Geol.* **2010**, *272*, 99–113.
36. Schwalenberg, K.; Wood, W.; Pecher, I.; Hamdan, L.; Stuart, S.; Jegen, M.; Coffin, R. Preliminary interpretation of electromagnetic, heat flow, seismic and geochemistry data for gas hydrate distribution across the Porangahau Ridge, New Zealand. *Mar. Geol.* **2010**, *272*, 89–108.
37. Hamdan, L.J.; Gillevet, P.M.; Pohlman, J.P.; Sikaroodi, M.; Greinert, J.; Coffin, R.B. Diversity and biogeochemical structuring of bacterial communities across the Porangahau ridge accretionary prism, New Zealand. *FEMS Microbiol. Ecol.* **2011**, *77*, 518–532.
38. Barnes, P.M.; Lamarche, G.; Bialas, J.; Henrys, S.A.; Pecher, I.A.; Netzeband, G.; Greinert, J.; Mountjoy, J.J.; Pedley, K.; Crutchley, G. Tectonic and geological framework for gas hydrates and cold seeps on the hikurangi subduction margin, New Zealand. *Mar. Geol.* **2010**, *272*, 26–48.

39. Katz, H.R. Probable gas hydrate in continental slope east of the North Island, New Zealand. *J. Pet. Geol.* **1981**, *3*, 315–324.
40. Pecher, I.A.; Henrys, S.A. *Potential Gas Reserves in Gas Hydrate Sweet Spots on the Hikurangi Margin, New Zealand*; Institute of Geological & Nuclear Sciences: Wellington, New Zealand, 2003.
41. Lewis, K.B.; Pettinga, J.R. The emerging imbricate frontal wedge of the Hikurangi margin. In *South Pacific Sedimentary Basins*; Balance, P.F., Ed.; Elsevier: Amsterdam, The Netherlands, 1993; pp. 225–250.
42. Hoehler, T.M.; Borowski, W.S.; Alperin, M.J.; Rodriguez, N.M.; Paull, C.K. Model, stable isotope, and radiocarbon characterization of anaerobic methane oxidation in gas hydrate-bearing sediments of the Blake Ridge. In Proceedings of the Ocean Drilling Program, Scientific Results, College Station, TX, USA, 2000; Volume 164, pp. 79–85.
43. Cline, J.D. Spectrophotometric determination of hydrogen sulfide in natural waters. *Limnol. Oceanogr.* **1969**, *14*, 454–459.
44. Plummer, R.E.; Pohlman, J.W.; Coffin, R.B. Compound-specific stable carbon isotope analysis of low-concentration complex hydrocarbon mixtures from natural gas hydrate systems. In Proceedings of AGU Fall Meeting Abstracts, San Francisco, CA, USA, 5–9 December 2005.
45. Osburn, C.L.; St-Jean, G. The use of wet chemical oxidation with high-amplification isotope ratio mass spectrometry (WCO-IRMS) to measure stable isotope values of dissolved organic carbon in seawater. *Limnol. Oceanogr. Meth.* **2007**, *5*, 296–308.
46. Borowski, W.S.; Paull, C.K.; Ussler, W., III. Carbon cycling within the upper methanogenic zone of continental rise sediments: An example from the methane-rich overlying the Blake Ridge gas hydrate deposits. *Mar. Chem.* **1997**, *57*, 299–311.
47. Aller, R.C.; Blair, N.E. Carbon remineralization in the Amazon-Guianas tropical mobile mudbelt: A sedimentary incinerator. *Cont. Shelf Res.* **2006**, *26*, 2241–2259.
48. Aller, R.C.; Blair, N.E.; Brunskill, G.J. Early diagenetic cycling, incineration, and burial of sedimentary organic carbon in the central Gulf of Papus (Papua New Guinea). *J. Geophys. Res.* **2008**, *113*, doi:10.1029/2006JF000689.
49. Martin, W.R.; McNichol, A.P.; McCorkle, D.C. The radiocarbon age of calcite dissolving at the sea floor: Estimates from pore water data. *Geochem. Cosmochim. Acta* **2000**, *64*, 1391–1404.
50. Sayles, F.L.; Curry, W.B. $\delta^{13}C$, TCO_2, and the metabolism of organic-carbon in deep-sea sediments. *Geochem. Cosmochim. Acta* **1988**, *52*, 2963–2978.
51. Macko, S.A.; Ostrom, N.E. Pollution studies using stable isotopes. In *Stable Isotopes in Ecology and Environmental Science*; Lajtha, K., Michener, R., Eds.; Blackwell Scientific Publications: Oxford, UK, 1994; pp. 45–62.
52. Martens, C.S.; Berner, R.A. Methane production in interstitial waters of sulfate-depleted marine sediments. *Science* **1974**, *185*, 1167–1169.
53. Whiticar, M. Carbon and hydrogen isotope systematics of bacterial formation and oxidation of methane. *Chem. Geol.* **1999**, *161*, 291–314.
54. Boetius, A.; Ravenschlag, K.; Schubert, C.J.; Rickert, D.; Widdel, F.; Gleske, A.; Amann, R.; Jørgensen, B.B.; Witte, U.; Pfannkuche, O. A marine microbial consortium apparently mediating anaerobic oxidation of methane. *Nature* **2000**, *407*, 623–626.

55. Meister, P.; Liu, B.; Ferdelman, T.G.; Jørgensen, B.B.; Khalili, A. Control of sulphate and methane distributions in marine sediments by organic matter reactivity. *Geochim. Cosmochim. Acta* **2013**, *104*, 183–193.
56. Berner, R.A. Sulfate reduction and the rate of deposition of marine sediments. *Earth Planet. Sci. Lett.* **1978**, *37*, 492–498.
57. Ussler, W., III.; Paull, C.K. Rates of anaerobic oxidation of methane and authigenic carbonate mineralization in methane-rich deep-sea sediments inferred from models and geochemical profiles. *Earth Planet. Sci. Lett.* **2008**, *266*, 271–287.
58. Claypool, G.E.; Milkov, A.V.; Lee, Y.-J.; Torres, M.E.; Borowski, W.S.; Tomaru, H. Microbial Methane Generation and Gas Transport in Shallow Sediments of Accretionary Complex, Southern Hydrate Ridge (ODP Leg 204), Offshore Oregon, USA. Available online: http://ir.library.oregonstate.edu/xmlui/handle/1957/13714 (accessed on 12 August 2014).
59. Claypool, G.E.; Kaplan, I.R. The origin and distribution of methane in marine sediments. In *Natural Gases in Marine Sediments*; Kaplan, I.R., Ed.; Plenum Press: New York, NY, USA, 1974; pp. 99–139.
60. Malinverno, A.; Pohlman, J.W. Modeling sulfate reduction in methane hydrate-bearing continental margin sediments: Does a suflate-methane transition require anaerobic oxidation of methane? *Geochem. Geophys. Geosyst.* **2011**, *12*, doi:10.1029/2011GC003501.
61. Boehme, S.E.; Blair, N.E.; Chanton, J.P.; Martins, C.S. A mass balance of ^{13}C and ^{12}C in an organic-rich methane-producing marine sediment. *Geochim. Cosmochim. Acta* **1996**, *60*, 3835–3848.
62. Peterson, B.J.; Howarth, R.W.; Garritt, R.H. Multiple stable isotopes used to trace the flow of organic matter in estuarine food webs. *Science* **1985**, *277*, 1361–1363.
63. Law, C.S.; Nodder, S.D.; Mountjoy, J.J.; Marriner, A.; Orpin, A.; Pilditch, C.A.; Franz, P.; Thompson, K. Geological, hydrodynamic and biogeochemical variability of a New Zealand deep-water methane cold seep during an integrated three-year time-series study. *Mar. Geol.* **2010**, *272*, 189–208.
64. Morse, J.W.; Beazley, M.J. Organic matter in deepwater sediments of the Northern Gulf of Mexico and its relationship to the distribution of benthic organisms. *Deep-Sea Res. II* **2008**, *55*, 2563–2571.
65. Coffin, R.B.; Osburn, C.L.; Plummer, R.; Grabowski, K.S. Deep sediment methane incorporation into shallow sediment carbon pools in Atwater Valley, Texas-Louisiana Shelf, Gulf of Mexico. *Energies* **2014**, submitted.
66. Wegener, G.; Niewmann, H.; Elvert, M.; Hinrichs, K.-U.; Boetius, A. Assimilation of methane and inorganic carbon by microbial communities mediating the anaerobic oxidation of methane. *Environ. Microbiol.* **2008**, *10*, 2287–2298.
67. Nauhaus, K.; Albrecht, M.; Elvert, M.; Boetius, A.; Widdel, F. *In vitro* cell growth of marine archaeal-bacterial consortia during anaerobic oxidation of methane with sulfate. *Environ. Microbiol.* **2007**, *9*, 187–196.
68. Knittel, K.; Boetius, A. Anaerobic oxidation of methane: Progress with an unknown process. *Annu. Rev. Microbiol.* **2009**, *63*, 311–334.
69. Leak, D.J.; Dalton, H. Growth yields of methanotrophs. *Appl. Microbiol. Biotechnol.* **1986**, *23*, 470–476.

70. House, C.H.; Schopf, J.W.; Stetter, K.O. Carbon isotopic fractionation by Archaens and other thermophilic prokaryotes. *Org. Geochem.* **2003**, *34*, 345–356.
71. Zhang, C.L.; Fouke, B.W.; Bonheyo, G.T.; Peackock, A.D.; White, D.C.; Huang, Y.; Romanek, C.S. Lipid biomarkers and carbon-isotopes of modern travertine deposits (Yellowstone Natioinal Park, USA): Implications for biogeochemical dynamics in hot-spring systems. *Geochem. Cosmochim. Acta* **2004**, *68*, 3157–3169.
72. Quandt, L.; Gottschalk, G.; Ziegler, H.; Stichler, W. Isotope discrimination by photosynthetic bacteria. *REMS Microbiol. Lett.* **1977**, *1*, 125–128.
73. Preuß, A.; Schauder, R.; Fuchs, G.; Stichler, W. Carbon isotope fractionation by autotrophic bacteria with three different CO_2 fixation pathways. *Z. Naturforsch. J. Biosci.* **1989**, *44*, 397–402.
74. Manske, A.K.; Glaeser, J.; Kuypers, M.M.M.; Overmann, J. Physiology and phylogeny of green sulfur bacteria forming a monospecific phototrophic assemblage at a depth of 100 meters in the Black Sea. *Appl. Environ. Microbiol.* **2005**, *71*, 8049–8060.
75. Inagaki, F.; Nunoura, T.; Nakagawa, S.; Teske, A.; Lever, M.; Lauer, A.; Suzuki, M.; Takai, K.; Delwiche, M.; Colwell, F.S.; *et al.* Biogeographical distribution and diversity of microbes in the methane hydrate-bearing deep marine sediments on the Pacific Ocean Margin. *Proc. Natl. Acad. Sci.* **2006**, *103*, 2815–2820.
76. Aoshima, M.; Igarashi, Y. A novel oxalosuccinate-forming enzyme involved in the reductive carboxylation of 2-oxoglutarate in Hydrogenbacter thermophiles TK-6. *Mol. Microbiol.* **2006**, *62*, 748–759.
77. Goñi, M.A.; Ruttenberg, K.C.; Eglinton, T.I. A re-assessment of the sources and importance of land-derived organic matter in surface sediment from the Gulf of Mexico. *Geochem. Cosmochim. Acta* **1998**, *62*, 3055–3075.
78. Gordon, E.S.; Goñi, M.A. Controls on the distribution and accumulation of terrigenous organic matter in sediments from the Mississippi and Atchafalaya river margin. *Mar. Chem.* **2004**, *92*, 331–352.
79. Szynkiewicz, A.M.; Jedrysek, O.; Kurasiewicz, M. Carbon isotope effects during precipitation of barium carbonate: Implications for environmental studies. *Environ. Chem. Lett.* **2006**, *4*, 29–35.